Simulation of the atmospheric thermal circulation of a martian volcano using a mesoscale numerical model

Scot C. R. Rafkin, Magdalena R. V. Sta. Maria & Timothy I. Michaels

Department of Meteorology, San José State University, One Washington Square, San José, California 95117, USA

Mesoscale (<100 km) atmospheric phenomena are ubiquitous on Mars, as revealed by Mars Orbiter Camera images[1–3]. Numerical models provide an important means of investigating martian atmospheric dynamics, for which data availability is limited. But the resolution of general circulation models, which are traditionally used for such research, is not sufficient to resolve mesoscale phenomena[4–6]. To provide better understanding of these relatively small-scale phenomena, mesoscale models have recently been introduced[7–9]. Here we simulate the mesoscale spiral dust cloud observed over the caldera of the volcano Arsia Mons by using the Mars Regional Atmospheric Modelling System. Our simulation uses a hierarchy of nested models with grid sizes ranging from 240 km to 3 km, and reveals that the dust cloud is an indicator of a greater but optically thin thermal circulation that reaches heights of up to 30 km, and transports dust horizontally over thousands of kilometres.

The Mars Regional Atmospheric Modelling System (MRAMS) is derived from a widely used atmospheric simulation code for the Earth's atmosphere[10]. The core dynamics of the model are built around discretized primitive equations of the atmosphere that include non-hydrostatic processes and acoustic waves. The vertical coordinate (sigma-z) closely follows the terrain elevation at low levels, and gradually distorts with height to a horizontally flat surface. Two-way interactive nested computational grids allow higher resolution of physical processes over limited areas. The solution obtained on a nested grid is averaged back to the coarser parent grid so that larger-scale dynamics are influenced by smaller-scale processes.

Three improvements to the MRAMS code have been made for this study. First, a new algorithm was used to calculate the horizontal pressure gradient. This method greatly reduces the numerical instability that can occur in terrain-influenced sigma-z models with extremely steep topography. The addition of this code was a requirement for this study, given the topographic relief of the volcanic Tharsis region. Second, we added parameterizations to model the effect of topographic shadowing and slope angle on both the surface energy budget and the solar heating of the atmospheric column. This addition is also crucial for this simulation, because the solar heating varies significantly owing to large variations in Sun and slope geometry. The final improvement was the inclusion of a dust lifting parameterization[11]—the mass of lifted dust increases as surface wind stress increases, and is activated when surface wind stress exceeds 14 mN.

The simulation period was three martian days, starting at a solar longitude of 180° (the vernal equinox), which corresponds to the date the cloud was imaged (Fig. 1) by the Mars Orbiter Camera (MOC). Only the last martian day of data was used for this analysis in order to minimize issues related to model spin-up. There are four, two-way interactive nested grids roughly centred over Arsia Mons. The two outer grids cover most of the Tharsis region and resolve the volcanic peaks reasonably well (Fig. 2). Note that the height of Olympus Mons and Arsia Mons are respectively 19,550 m and 16,410 m on grid two of the model, whereas observations indicate heights of 21.3 km and 17.6 km, respectively. The topography on grid one is better resolved by at least a factor of two compared to a typical general circulation model (GCM). The domain of the third grid is slightly larger than Arsia Mons (not shown), and the fourth grid covers the caldera (Fig. 3). The horizontal grid spacing is respectively 240 km, 60 km, 15 km and 3 km for each of the nested grids. The nominal vertical grid spacing is 50 m in the lowest model level, and is stretched gradually to a maximum spacing of 1,200 m. The model top is at 60 km. The initial large-scale fields and time-dependent boundary conditions were supplied by simulation 9974 in the NASA Ames Mars General Circulation Model (MGCM) Climate Catalog. The model domain is nearly hemispheric in order to minimize the spurious influence of inaccurate boundary conditions[8]. Data from the last year of the two-year MGCM simulation was used for this purpose. The background dust concentration is fixed at an optical depth of 0.3 at 611 Pa. The lifted dust augments the background value, and total dust optical depth is used to calculate the radiative heating. The lifted dust is assumed to have a backscatter coefficient of 2.0, which is consistent with a particle diameter size of approximately 1 μm.

The MRAMS-simulated horizontal wind field at 24 m above ground level, and the vertically integrated dust mass, is shown in Fig. 3, which can be compared to the observed cloud (Fig. 1). Although the simulated dust cloud is off-centre from the caldera, there are notable similarities between the observed and simulated cloud, and we are confident that the model has captured the essential features of the observed cloud and the accompanying atmospheric circulation. The scale of the observed and simulated clouds are approximately the same, and the sense of rotation implied by the spiral formation in the observations agrees with the clockwise circulation in the simulation. The cloud was observed at approximately 14:00 local time, and was at an altitude between 10 km and 15 km above the caldera on the basis of viewing geometry and shadow length. The uncertainty results from the pixel resolution in the image. It is not known at what time the cloud became optically visible. The simulated cloud is well organized by 16:00 local time. The cloud top is approximately 15 km above ground, in agreement with the altitude computed by the shadow geometry. The

Figure 1 Mars Orbiter Camera image of a spiral dust cloud observed above the caldera of Arsia Mons. The pseudo-colour image was obtained by combining the red- and blue-filter MOC data. The original image was cropped to focus on the caldera, which is the faint, dark, ring towards the edge of the image. The cloud structure (the central, bright spiral) implies a clockwise and convergent circulation, and casts (to its right) a shadow on the caldera floor. Faint, white water ice clouds are also visible. The image should be compared with Fig. 3. Image reproduced with permission from Malin Space Science Systems.

simulated cloud is sufficiently dense to be visible through the red filter of the MOC. The spiral cloud did not form when an identically configured simulation was performed at a solar longitude of 142°. Consequently, the simulation indicates at least some seasonality to the circulation, which probably results either from changes in the thermal circulation due to changes in solar heating, or as a result in changes of the large-scale flow as predicted by the MGCM.

Although the dust cloud is visually captivating, the unseen thermal circulation predicted by MRAMS—and from which the spiral cloud originates—is of greater interest. A vertical cross-section (Fig. 4) reveals that the spiral dust cloud is the dense portion of a much larger, optically thin, mushroom-shaped dust cloud associated with the thermal circulation forced by Arsia Mons. Parcels of air originating near the base or along the slopes of Arsia Mons traverse a helical convergent path upwards, with a peak vertical ascent rate of several metres per second. There is sufficient energy for an air parcel rising along the slopes of the volcano to ascend to an altitude of 30 km above the reference geoid. Dust is preferentially lifted near the base of the mountain, where densities are higher and dust lifting mechanisms are more effective for a given wind speed. The origin of the dust in the observed cloud is not from within the caldera, but from along the lower slopes of the volcano. The convergent wind field concentrates the dust into the optically thick spiral cloud feature.

The flow becomes horizontally divergent near the top of the circulation, where the outflow branches of the circulation transport dust laterally up to a thousand or more kilometres on either side of the volcano. Owing to the lower density at higher altitudes, conservation of mass requires that the velocity of the diverging air greatly exceed the velocity of the low-level inflow. Wind speeds along the slopes of the volcano are in excess of 25 m s^{-1}, but 15 m s^{-1} is more typical. The outflow speed aloft exceeds 40 m s^{-1}. Dust undergoing horizontal transport in the outflow branches of the thermal circulation would, in reality, undergo size sorting by way of sedimentation. A dust particle of less than 1 μm in diameter falling at 1 cm s^{-1} would require in excess of 20 martian days to fall 20 km in altitude in the absence of vertical motion in the atmosphere. Such a particle could travel significant horizontal distances within this timeframe. Dust less than 1 μm in diameter would remain aloft for even longer periods, and could easily circle the planet given only the moderate wind speeds predicted by Mars GCMs.

The air in the rising branch of the thermal circulation is cooled adiabatically to temperatures as low as 135 K at an altitude of 30 km

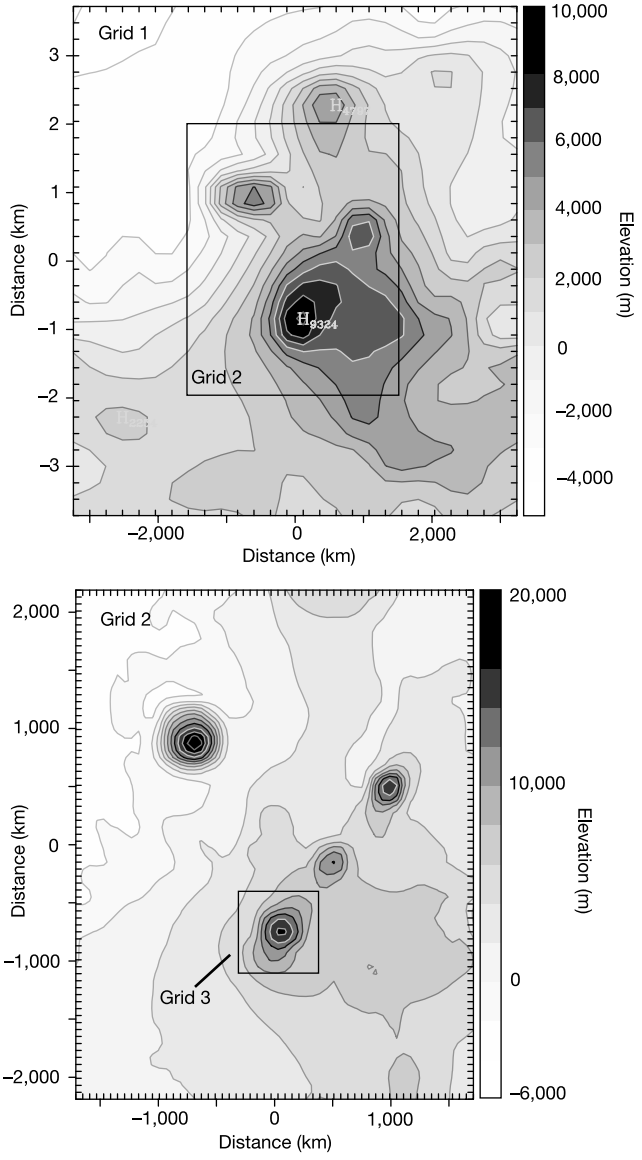

Figure 2 Topography and domain size for the first two computational grids. The horizontal grid spacing for grid 1 is 240 km, and for grid 2, 60 km. The rectangular boxes indicate the location of the next nested grid. The first grid has at least twice the topographic resolution of a typical GCM, and the Tharsis region volcanoes are only half their actual size at best. For grid 1, the minimum, maximum and contour interval for the topography is respectively 4,136 m, 9,324 m and 1,000 m. The second grid almost completely resolves the shape and height of the volcanic system. The minimum, maximum and contour interval for the topography on grid two is respectively −3,999 m, 19,550 m and 2,000 m. Grids three (rectangular box in grid two) and four (not shown) focus entirely on Arsia Mons, and allow the detailed simulation of the thermal circulation and the genesis of the spiral dust cloud. MRAMS properly represents the thermal circulations forced by the volcanoes, because the dimensions of the volcanoes are very near the actual values on the inner nested grids.

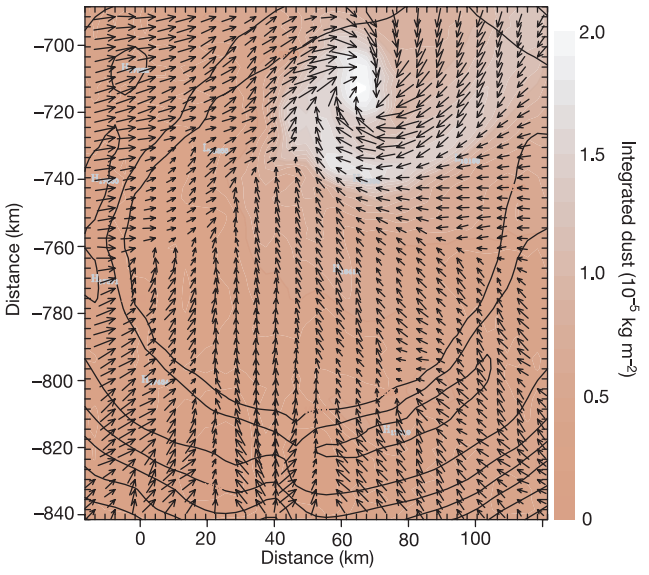

Figure 3 The spiral dust cloud simulated by the Mars Regional Atmospheric Modelling System (MRAMS), as seen on the fourth computational grid, which encompasses the caldera of Arsia Mons. Shading indicates the integrated dust mass per km^3. Solid contours indicate topography elevation. Vectors indicate wind speed and direction. The strongest wind speed is 42 m s^{-1}. The spiral cloud feature and winds reveal a clockwise, convergent circulation, with maximum dust concentration near its centre. This figure should be compared with the imaged dust cloud in Fig. 1.

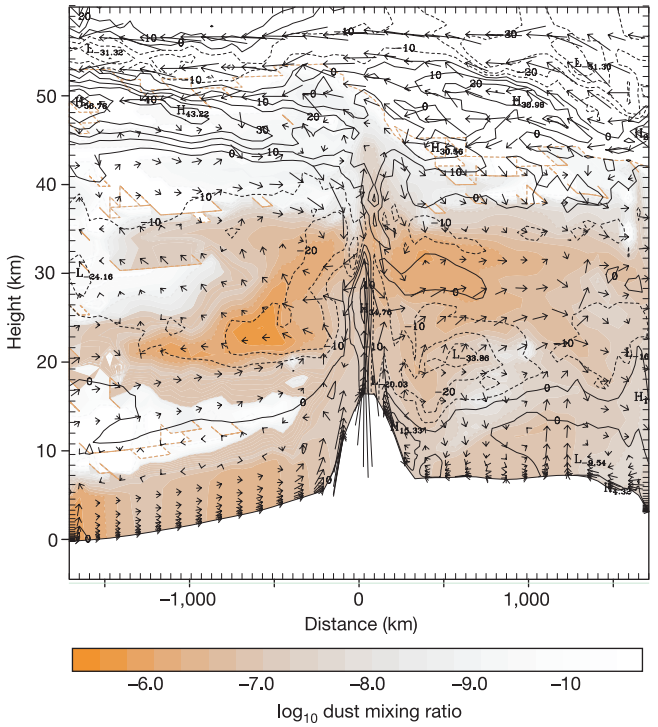

Figure 4 A vertical, east–west cross-section from grid two, cutting through the centre of Arsia Mons. Shaded regions are $\log_{10}$ of the dust mixing ratio. Contour lines indicate meridional wind: solid lines, northward-moving air (into the page); dotted lines, southward-moving air (out of the page). Vectors indicate wind velocity in the plane of the figure. The maximum horizontal wind speed is 95 m s^{-1}. The maximum vertical velocity is 9 m s^{-1}. The dust takes the form of a mushroom-shaped cloud. The upper-level outflow from the thermal circulation advects the dust more than 2,000 km downwind. The meridional wind shows a tight clockwise rotation directly above the caldera. The outflow region to either side of the volcano exhibits a weaker anticlockwise rotation.

(not shown). It would not be unexpected for a water-ice cloud to develop at the top of the thermal circulation. Such cap clouds have been observed by the MOC and by the Viking orbiter[12]. But the actual amount of water vapour in the air is unknown, so we chose to run the model without the presence of any water substance in this study.

The GCMs that are typically used to study the climate of Mars have too coarse a grid spacing to properly resolve Arsia Mons (or the other volcanoes, all of which exhibit similar circulations), and are therefore unable to capture the magnitude of the thermal circulation or the dust injection mechanism associated with the circulations. These same models would not properly reproduce the radiative balance of the atmosphere, as they would not reproduce the dust loading. The easterly winds in the outflow branch (Fig. 4) effectively enhance the depth of the upper-level large-scale easterly winds. Westerly winds in the outflow located below the large-scale upper-level easterly winds increase the wind shear. Consequently, the thermal circulation creates a large perturbation in the larger-scale momentum and thermal fields.

Mars is dotted with numerous topographic features that are too small in horizontal extent to be captured by GCMs, but which may produce large-scale thermal circulations that could perturb the general circulation. Our results suggest that mesoscale thermal circulations may collectively be important in the atmospheric dust budget, and individually can produce strong regional perturbations in the background large-scale flow. □

Received 10 April; accepted 10 September 2002; doi:10.1038/nature01114.

1. Cantor, B., Malin, M. & Edgett, K. S. Multiyear Mars Orbiter Camera (MOC) observations of repeated Martian weather phenomena during the northern summer season. *J. Geophys. Res.* **107,** 10.1029/2001JE001588 (2002).
2. Cantor, B. A., James, P. B., Caplinger, M. & Wolff, M. J. Martian dust storms: 1999 Mars Orbiter Camera observations. *J. Geophys. Res.* **106,** 23653–23687 (2002).
3. Malin, M. C. & Edgett, K. S. Mars Global Surveyor Mars Orbiter Camera: Interplanetary cruise through primary mission. *J. Geophys. Res.* **106,** 23429–23570 (2001).
4. Haberle, R. M. *et al.* General circulation model simulations of the Mars Pathfinder atmospheric structure investigation/meteorology data. *J. Geophys. Res.* **104,** 8597–8974 (1999).
5. Wilson, R. J. & Hamilton, K. Comprehensive model simulation of thermal tides in the Martian atmosphere. *J. Atmos. Sci.* **53,** 1290–1326 (1996).
6. Forget, F. *et al.* Improved general circulation models of the Martian atmosphere from the surface to above 80 km. *J. Geophys. Res.* **104,** 24155–24175 (1999).
7. Rafkin, S. C. R., Haberle, R. M. & Michaels, T. I. The Mars Regional Atmospheric Modeling System (MRAMS): Model description and selected simulations. *Icarus* **151,** 228–256 (2001).
8. Tyler, D., Barnes, J. R. & Haberle, R. M. Simulation of surface meteorology at the Pathfinder and VL1 sites using a Mars mesoscale model. *J. Geophys. Res.* 10.1029/2001JE001618 (2002).
9. Toigo, A. D. & Richardson, M. I. A mesoscale model for the Martian atmosphere. *J. Geophys. Res.* **107,** 10.1029/2001JE001489 (2002).
10. Pielke, R. A. *et al.* A comprehensive meteorological modeling system—RAMS. *Meteorol. Atmos. Phys.* **49,** 69–91 (1992).
11. Murphy, J. R., Haberle, R. M., Toon, O. B. & Pollack, J. B. Martian global dust storms: Zonally symmetric numeric simulations including size-dependent particle transport. *J. Geophys. Res.* **98,** 3197–3220 (1993).
12. Hunt, G. E., Pickersgill, A. O., James, P. B. & Johnson, G. Some diurnal properties of clouds over the martian volcanoes. *Nature* **286,** 362–364 (1980).

Acknowledgements We thank Malin Space Science Systems and M. Malin for permitting the use of MOC imagery before release on Planetary Data System. We also thank A. Bridger for comments and suggestions. This work was supported by the NASA Planetary Atmosphere Program, the Mars Data Analysis Program and the Mars Global Surveyor Data Analysis Program.

Competing interests statement The authors declare that they have no competing financial interests.

Correspondence and requests for materials should be addressed to S.C.R.R. (e-mail: rafkin@metsun1.met.sjsu.edu or srafkin@boulder.swri.edu).

Cavity solitons as pixels in semiconductor microcavities

Stephane Barland*¶, Jorge R. Tredicce*¶, Massimo Brambilla†¶, Luigi A. Lugiato‡, Salvador Balle§, Massimo Giudici*, Tommaso Maggipinto†, Lorenzo Spinelli‡, Giovanna Tissoni‡, Thomas Knödl‖, Michael Miller‖ & Roland Jäger‖

* *Institut Non Lineaire de Nice, 1361 Route des Lucioles, F-06560 Valbonne, France*
† *INFM, Dipartimento di Fisica Interateneo, Poltecnico e Università di Bari, Via Orabona 4, 70126 Bari, Italy*
‡ *INFM, Dipartimento di Scienze, Università dell'Insubria, Via Valleggio 11, 22100 Como, Italy*
§ *IMEDEA, Carrer Miguel Marques 21, 07190 Esporles, Islas Baleares, Spain*
‖ *Department of Optoelectronics, University of Ulm, Albert-Einstein-Allee 45, D-89069 Ulm, Germany*
¶ *These authors contributed equally to this work*

Cavity solitons are localized intensity peaks that can form in a homogeneous background of radiation. They are generated by shining laser pulses into optical cavities that contain a nonlinear medium driven by a coherent field (holding beam). The ability to switch cavity solitons on and off[1,2] and to control their location and motion[3] by applying laser pulses makes them interesting as potential 'pixels' for reconfigurable arrays or all-optical processing units. Theoretical work on cavity solitons[2–7] has stimulated a variety of experiments in macroscopic cavities[8–10] and in systems with optical feedback[11–13]. But for practical devices, it is desirable to generate cavity solitons in semiconductor structures, which